Am J Cancer Res 2024;14(8):3905-3921
www.ajcr.us /ISSN:2156-6976/ajcr0158249

Original Article

Cucurbitacin E elicits apoptosis in laryngeal squamous cell carcinoma by enhancing reactive oxygen species-regulated mitochondrial dysfunction and endoplasmic reticulum stress

Xucai Zheng[1,4], Puze Tang[2], Hui Li[3], Tingbo Ye[4], Xu Zhu[3], Wei He[3], Ling Cheng[5], Huaidong Cheng[1,6]

[1]Department of Oncology, The Second Hospital of Anhui Medical University, Hefei 230601, Anhui, China; [2]Bachelor of Science in Mathematics, University of Liverpool, United Kingdom; [3]Department of Immunology, School of Basic Medical Sciences, Anhui Medical University, Hefei 230032, Anhui, China; [4]Department of Head, Neck and Breast Surgery, The First Affiliated Hospital of USTC, Anhui Provincial Cancer Hospital, Hefei 230031, Anhui, China; [5]Medical Intensive Care Unit, The First Affiliated Hospital of Anhui University of Chinese Medicine, Hefei 230031, Anhui, China; [6]Department of Oncology, Shenzhen Hospital of Southern Medical University, Shenzhen 518000, Guangdong, China

Received June 4, 2024; Accepted August 18, 2024; Epub August 25, 2024; Published August 30, 2024

Abstract: Laryngeal squamous cell carcinoma (LSCC) is a prevalent head and neck neoplasm with escalating global morbidity and mortality rates. Despite the increasing burden of LSCC, the drugs currently approved for its treatment are limited. Therefore, it is necessary to identify novel and promising drugs that target LSCC. Cucurbitacin E (CuE) is a naturally oxygenated tetracyclic triterpenoid that suppresses several cancers. However, its anti-LSCC activity and the molecular mechanisms of action remain unclear. This study explored its impact on LSCC, revealing cell viability attenuation and apoptosis enhancement *in vitro*. Further investigations indicated that CuE significantly decreased mitochondrial membrane potential, thereby promoting cytochrome c release, increasing cleaved-Caspase 3 and cleaved-PARP levels, and triggering mitochondria-dependent apoptosis. Concurrently, exposure of LSCC cells to CuE enhanced endoplasmic reticulum (ER) stress, mobilized the protein kinase RNA-like endoplasmic reticulum kinase/initiation factor 2a/ATF4/C-EBP homologous protein pathway, and induced LSCC cell apoptosis. Finally, CuE markedly elevated intracellular reactive oxygen species (ROS) levels. When ROS were eliminated with N-acetylcysteine, CuE-mediated mitochondrial dysfunction, ER stress, and cell apoptosis were nearly abolished. Similar outcomes were observed in murine LSCC models. Together, these results highlight that CuE suppresses proliferation while triggering apoptosis in LSCC cells via ROS-regulated mitochondrial dysfunction and the ER stress pathway. Hence, CuE may serve as a promising candidate for LCSS treatment.

Keywords: Cucurbitacin E, laryngeal squamous cell carcinoma, mitochondrial dysfunction, reactive oxygen species, endoplasmic reticulum stress

Introduction

Laryngeal squamous cell carcinoma (LSCC), a prevalent head and neck neoplasm, has become one of the leading cancers globally, with an annual increase of 25% [1]. Despite noticeable progress in diagnosis and treatment, approximately 60% of patients with LSCC are still diagnosed at a late stage (III or IV) [2, 3]. This late diagnosis often results in a missed opportunities for surgical intervention, contributing to a decreased 5-year survival rate for patients with LSCC in recent decades [4, 5]. Therefore, exploring novel and promising drug candidates for LSCC treatment is urgently needed.

Cucurbitacin E (CuE), originally extracted from *Cucumis melo L*, is a natural tetracyclic triterpenoid [6]. This biochemical compound possesses multiple pharmacological properties, including anti-diabetic, anti-tumor, and anti-inflammatory effects [7, 8]. Numerous studies have demonstrated the ability of CuE to inhibit the malignant progression of gastric, live, and lung cancers [8-10]. CuE influences many tumor

https://doi.org/10.62347/HPQQ9412

cell phenotypes, including proliferation, metastasis, apoptosis, cell cycle, senescence, autophagy, and chemo-response [6, 8, 9, 11-13]. However, the specific functions and molecular mechanisms underlying LSCC remain to be elucidated.

The endoplasmic reticulum (ER) is a central location for protein, lipid, and sugar synthesis and protein folding in eukaryotic cells [14]. Exposure to cancerous cells, oxidative stress, toxic drugs, and radiation can lead to an increase in unfolded and misfolded protein aggregations in the ER lumen, resulting in ER stress [15, 16]. Sustained and drastic ER stress can activate protein kinase RNA-like endoplasmic reticulum kinase (PERK), leading to increase in initiation factor 2a (eIF2a) phosphorylation, subsequent ATF4 and C/EBP homologous protein (CHOP) translation, proliferation arrest, and apoptosis [17]. Substantial evidence has shown that immoderate reactive oxygen species (ROS) lead to oxidative stresses, triggering misfolded protein accumulation in the ER lumen and resulting in ER stress [18, 19]. Meanwhile, excessive ROS overproduction can affect mitochondrial structure and function, causing a reduction in mitochondrial membrane permeability and ultimately leading to cell apoptosis [20, 21]. Recent reports have demonstrated that CuE induces cancer cell death by increasing ROS production [12, 22]. However, whether CuE-induced ROS generation triggers ER stress-regulated signaling pathways, mitochondrial dysfunction, and ultimately LSCC cell apoptosis is not completely understood.

In this study, we evaluated the anti-LSCC functions of CuE and investigated the roles of ROS generation-regulated ER stress and mitochondrial dysfunction in the modulation of CuE-induced LSCC cell apoptosis. Our findings offer new insights into the molecular mechanisms of action of CuE against LSCC and demonstrate the potential of CuE in LSCC treatment.

Materials and methods

Reagents

Thr ROS scavenger N-acetylcysteine (NAC, HY-B0215), CuE (HY-N0417), and the ER stress inhibitor 4-phenylbutyric acid (4-PBA, HY-A0281) were purchased from MedChemExpress. The pan-caspase inhibitors carbobenzoxy-valyl-alanyl-aspartyl-[O-methyl]-fluoromethylketone (Z-VAD-FMK) and dimethyl sulfoxide (DMSO, D8418) were obtained from TopScience (Shanghai, China) and Sigma-Aldrich (St. Louis, MO, USA), respectively.

Cell cultivation

LSCC cells, TU686 (BeNa Culture Collection, Beijing, China) and AMC-HN-8 (ATCC, USA), were cultivated in high-glucose DMEM (Biosharp, Hefei, China) with 10% FBS (Wisent, Canada) and 1% penicillin/streptomycin (Beyotime, Shanghai, China) at 37°C with 5% CO_2.

Cell viability assay

To examine the effects of CuE on cell viability, LSCC cells (2×10^3 cells/well) were seeded in 96-well plates. Different concentrations of CuE (0.05, 0.1, 0.2, 0.4 μM) dissolved in DMSO were added into the culture medium. After incubation for various periods, cell viability was quantified using the CCK-8 assay (TopScience, C0005) as previously reported [23].

Colony formation assay

LSCC cells (2×10^3 cells/well) were cultured overnight in 6-well plates and treated with CuE at different doses for 2 weeks, with the medium refreshed every 4 days. Subsequently, colony formation was assessed by staining with crystal violet (Beyotime, C0121) after incubation with 4% paraformaldehyde, followed by photographing using a scanner (Hewlett-Packard, Palo Alto, CA, USA), and counting using ImageJ software (NIH, USA).

Morphological observation

Following 24 h of CuE treatment at various concentrations, morphological changes in LSCC cells were recorded using a Leica DFC7000 T microscope Cameras (Leica Microsystems, Wetzlar, Germany).

Annexin V/PI staining

LSCC cells (5×10^5/well) in 6-well plates were incubated with CuE at various doses for 24 h with or without 4-PBA, NAC, or Z-VAD-FMK after 12 h of culture. The cells were then collected and labeled with FITC-Annexin V/PI, as indicated by the manufacturer (BestBio, BB-4101,

Table 1. Antibody list

Antibody	Dilution	Vendor	Catalogue Number
Caspase 3	1:1000	Selleck	Cat. No. A5185
C-Caspase 3	1:1000	Huabio	Cat. No. ET1602-47
PARP	1:1000	Zenbio	Cat. No. R25279
Cytochrome c	1:1000	Selleck	Cat. No. A5184
p-PERK	1:1000	Zenbio	Cat. No. 340846
PERK	1:1000	Zenbio	Cat. No. R25331
p-eIF 2α	1:1000	Selleck	Cat. No. A5941
eIF 2α	1:1000	Zenbio	Cat. No. 340347
ATF4	1:1000	Selleck	Cat. No. A5514
CHOP	1:1000	Selleck	Cat. No. A5462
α-Tubulin	1:5000	Zenbio	Cat. No. 250009
Goat Anti-Rabbit IgG/HRP	1:5000	Zenbio	Cat. No. 511203
Goat Anti-mouse IgG/HRP	1:5000	Zenbio	Cat. No. 511103

Shanghai, China). Apoptotic cells were detected with a CytoFLEX cytometer (Beckman Coulter, Brea, CA, USA), and the fraction of apoptotic cells was measured using CytExpert software.

Mitochondrial membrane potential (MMP) assay

Variations in MMP levels were determined using a JC-1 assay kit (C2006; Beyotime, China). LSCC cells (3 × 10^5/well) were treated with CuE (0.05, 0.1, 0.2 μM) for 24 h after incubating overnight in 12-well plates. Subsequently, cells were washed three times with 1 × phosphate buffer saline (PBS), and reacted with JC-1 staining solution for 15 min at 37°C. Then, the supernatant containing JC-1 was removed, and the cells were washed three times with JC-1 staining buffer. After adding 2 ml cell culture medium, the cells were examined and photographed using the aforementioned-mentioned Microscope Cameras.

ROS measurement

ROS levels in LSCC cells were assessed using Dichloro-dihydro-fluorescein diacetate (DCFH-DA) (S0033M; Beyotime, China). Cells (5 × 10^5/well) in 6-well plates were cultivated overnight, treated with CuE at various dosages for 24 h, washed with 1 × Hank's Balanced Salt Solution, and stained with 10 μM DCFH-DA in non-FBS DMEM at 37°C for 20 min. Subsequently, the cells were sorted through flow cytometry and analyzed using CytExpert software.

Measurement of ER expansion

LSCC cells were cultured in 6-well plates with varying doses of CuE for 24 h with or without NAC. Subsequently, the cells were incubated with ER-Tracker Red (Beyotime, China, C1041S) for 30 min according to the manufacturer's instructions, and ER stress was examined using a microscope cameras (Leica DFC7000 T, Leica Microsystems, Wetzlar, Germany).

Western blotting

Cells and tumor tissues were lysed on ice for 45 min in RIPA buffer (P0013B) containing protease (P1005) and phosphatase inhibitors (P1045) procured from Beyotime, China. The lysates were cleared by spinning at 12000 rpm for 30 min at 4°C, subjected to 12% SDS-PAGE after measuring concentration with the BCA Protein Assay Kit (Beyotime, China, P0012S), electro-separated on gels, and transferred onto nitrocellulose membranes (BioTrace™ NT Membrane, Pall Corporation, Ann Arbor, MA). After incubation with 5% fat-free milk and overnight treatment with primary antibodies at 4°C under gentle shaking, the membranes were rinsed with 1 × PBST (0.1% Tween-20 in PBS) and reacted with secondary antibodies for 2 h at ambient temperature. Protein signals were detected using chemiluminescence detection (Tanon, Shanghai, China) on a Tanon-5200 instrument (Tanon, Shanghai, China) and analyzed using ImageJ software (NIH, USA). **Table 1** lists all the antibodies used.

Mouse xenograft model

All animal procedures were approved by the Animal Welfare Committee and the Institutional Animal Care and Use Committee of the Anhui Medical University Laboratory Animal Center and were implemented in compliance with the protocol of the Animal Ethics Committee (approval No. 20240920). Healthy female BALB/c nude mice at 5 weeks old (GemPharmatech, Nanjing, China) were accommodated in a pathogen-free condition with a suitable environment (23 ± 2°C, 50 ± 5% humidity, 12 h light/dark cycle), and the ani-

mals were provided with free access to food and water. After a 7-day acclimation period, 100 μL of 1 × 10^6 TU686 cells in PBS were administrated subcutaneously into the left armpit. Once tumors were formed, tumor-bearing mice were randomly grouped, and 100 μl of PBS, 1% DMSO in PBS, and 5 or 10 mg/kg CuE (dissolved in DMSO and diluted using PBS) were intraperitoneally administered every other day. Tumor volume was assessed every 4 days and determined as length × $(width)^2$ × 0.5. Mice were euthanized using pentobarbital three weeks later. Tumors were collected, weighed, dissected into several pieces, and either stored at -80°C for western blotting or in 4% paraformaldehyde for staining.

Tissue staining

Haematoxylin and eosin (H&E) staining was performed using an H&E staining kit (G1120, Solarbio, Beijing, China) according to the manufacturer's protocol. Tumor, heart, kidney, spleen, liver, and lung tissues from the mice in each group were fixed with 4% paraformaldehyde for 48 h, embedded in paraffin and sectioned into 5-μm sections. After dewaxing with xylene and rehydrating with an ethanol gradient, the slices were stained with hematoxylin and eosin. Subsequently, the slices were dehydrated and sealed. Each slice was then analyzed using a microscope cameras (Leica DFC7000 T; Leica Microsystems, Wetzlar, Germany).

Terminal-deoxynucleotidyl transferase-mediated deoxyurine triphosphate (d-UTP) nick end labeling (TUNE) staining was performed using the one-step TUNEL Apoptosis Assay Kit (C1086, Beyotime) was employed following the manufacturer's protocol. Xenograft tumor tissue slices were removed wax in xylene and rehydrated with an ethanol gradient. The slices were then incubated with the protease K at 37°C for 20 min and washed three times with 1 × PBS. Subsequently, the slices were dealt with TUNEL test solution for 1 h, followed by staining with 4,6-diamidino-2 phenylindole (DAPI) for 2 min at 37°C in the dark, and mounted using an anti-fade Mounting Medium (P0128S, Beyotime). Images were captured using a laser scanning confocal microscope (Zeiss LSM 880 with Airyscan).

Statistical analysis

Data were normally distributed, presented as average ± standard deviation (SD), and displayed using GraphPad Prism 8 (GraphPad Software Inc., USA). Differences were assessed using one-way ANOVA with Dunnett's tests or post-hoc Bonferroni correction for multiple groups and an unpaired, two-tailed *t*-test for comparisons between two groups. Statistical significance was set at $P < 0.05$; ns indicates no statistical difference.

Results

CuE suppresses human LSCC cell growth

To assess the influence of CuE on the viability of LSCC cells, TU686 and AMC-HN-8 cells were reacted with varying dosages of CuE (0.05-0.4 μM) for 24, 48, and 72 h. CCK-8 analysis revealed a remarked concentration-dependent and time-dependent reduction in the viability of CuE-treated LSCC cells compared to DMSO-treated LSCC cells (**Figure 1A**, **1B**). Additionally, colony formation assay revealed that CuE treatment reduced colony numbers in a concentration-dependent manner, with the most notable inhibition at 0.2 μM (**Figure 1C**, **1D**). These findings suggested that CuE suppressed the growth of human LSCC cells.

CuE induces caspase-dependent LSCC cell apoptosis

To elucidate the underlying mechanism of action of CuE in LSCC cells, we examined its effects on LSCC cell morphology. **Figure 2A** illustrates that CuE treatment resulted in TU686 and AMC-HN-8 cell rounding and detachment, with the round cell numbers escalating proportionately with increasing CuE dosage. Next, we ascertained the fraction of apoptotic cells using flow cytometry after Annexin V-FITC/PI staining. Exposure to CuE for 24 h in a dose-dependent manner augmented the proportion of apoptotic cells in both TU686 and AMC-HN-8 cells (**Figure 2B**, **2C**). Furthermore, Western blotting revealed that CuE treatment dose-dependently increased cleaved-Caspase 3 and cleaved-PARP (C-Caspase 3/PARP) levels in LSCC cells (**Figure 2D**, **2E**). To examine the involvement of caspases in CuE-triggered apoptosis, TU686 and AMC-HN-8

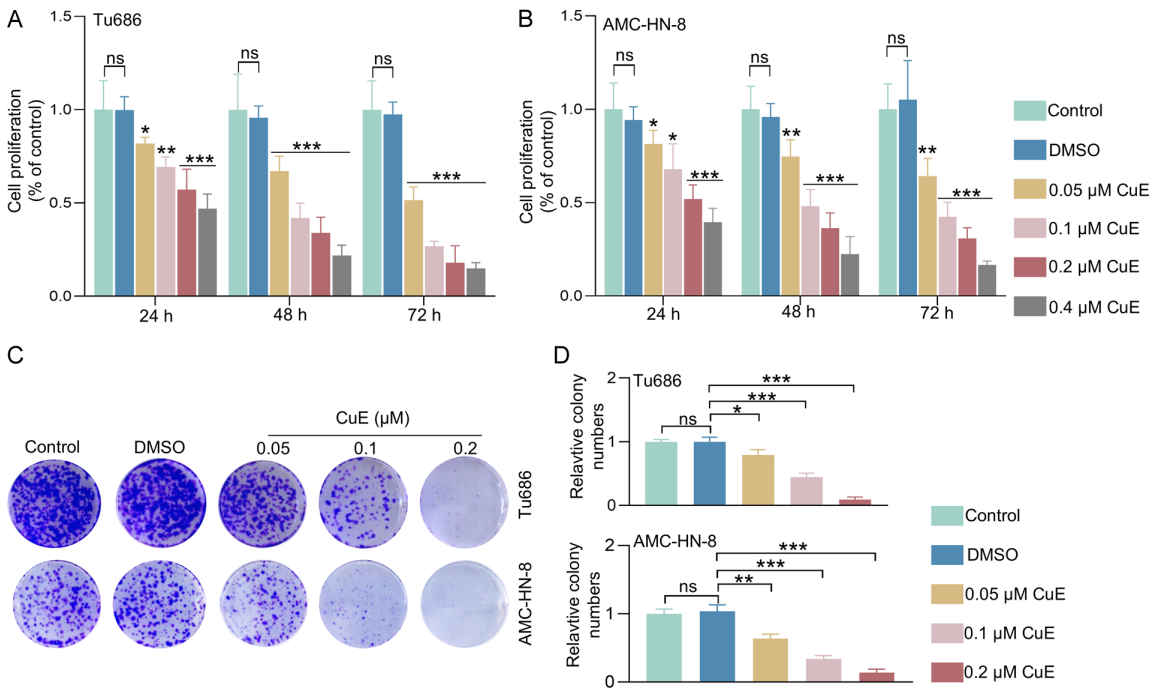

Figure 1. CuE attenuated LSCC cell viability. A, B. LSCC cell viability was quantified using the CCK-8 assay after incubation with CuE at varying doses for 24, 48, and 72 h. C, D. The number of colonies formed after incubation with CuE at various concentrations for 14 days, as examined via crystal violet staining. Data are shown as means ± SD (n=3). *, **, and *** indicate $P < 0.05$, 0.01, and $P < 0.001$ *vs.* the DMSO group, respectively. ns, no significance.

cells were preincubated with Z-VAD-FMK for 1 h before CuE (0.1 μM) treatment. These results indicate that Z-VAD-FMK preincubation markedly reversed CuE-triggered LSCC cell apoptosis (**Figure 3A**, **3B**). Consistently, C-Caspase 3/PARP levels were downregulated in CuE-treated LSCC cells after Z-VAD-FMK pretreatment (**Figure 3C**, **3D**). These results demonstrated that CuE-induced LSCC cell growth inhibition was mediated by caspase-induced apoptosis.

CuE fosters apoptosis via the mitochondrial pathway in LSCC cells

Mitochondrial dysfunction contributes to cellular apoptosis. To investigate whether CuE-induced apoptosis involves the mitochondria, we examined the MMP of LSCC cells using the JC-1 assay. CuE treatment for 24 h markedly increased green fluorescence and decreased red fluorescence in both TU686 and AMC-HN-8 cells (**Figure 4A**). The green-to-red signal ratio increased in LSCC cells, indicating that CuE decreased the MMP of these cells. This alteration may promote cytochrome c release from the mitochondria, thereby activating the caspases-dependent apoptotic pathway. Interestingly, CuE dose-dependently increased cytoplasmic cytochrome c levels in LSCC cells (**Figure 4B**, **4C**), which was consistent with the finding that CuE treatment augmented C-Caspase 3/PARP levels in both TU686 and AMC-HN-8 cells (**Figure 2D**, **2E**). These findings revealed that CuE induced LSCC cell apoptosis via the mitochondria-related apoptotic pathway.

ER stress regulates CuE-triggered LSCC cell apoptosis

To investigate whether CuE triggers apoptosis by activating ER stress, we examined ER stress in LSCC cells using an ER-ID® Red assay. CuE treatment increased the fluorescence intensity of both TU686 and AMC-HN-8 cells in a dose-dependent manner (**Figure 5A**). We further examined changes in phospho-PKR-like ER kinase (p-PERK) and phospho-eukaryotic initiation factor-2α (p-eIF2α)/ATF-4/CHOP after subjecting to various doses of CuE for 24 h. Compared to DMSO, CuE significantly upregulated p-PERK, p-eIF2α, ATF-4, and CHOP protein levels in LSCC cells, indicating that CuE

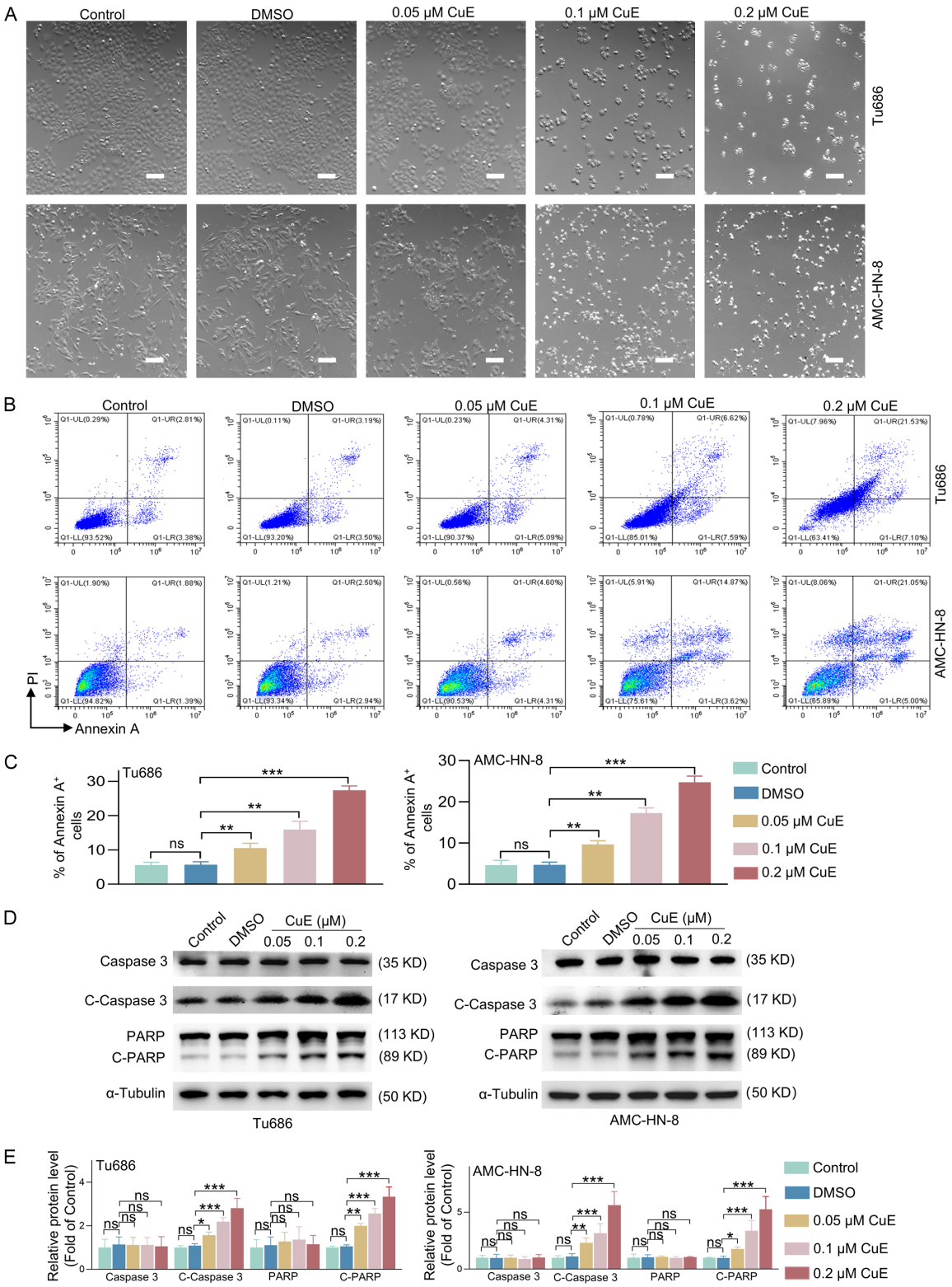

Figure 2. CuE triggered the caspase-dependent LSCC cell apoptosis. A. Changes in LSCC cell morphology after CuE treatment at the indicated concentrations. Scale bar =100 μm. B, C. The fraction of apoptotic LSCC cells after CuE treatment at varying doses for 24 h and staining with Annexin V/PI staining, as evaluated using flow cytometry. D, E. Western blotting of C-Caspase 3/PARP in LSCC cells conditioned with 0.05, 0.1, and 0.2 μM CuE for 24 h, and the intensity of protein bands was quantified using by Image J. C-Caspase 3/PARP, cleaved-Caspase 3 and cleaved-PARP. Data are presented as means ± SD (n=3). *, **, and *** indicate $P < 0.05$, 0.01, and $P < 0.001$ *vs.* the DMSO group, respectively. ns, no significance.

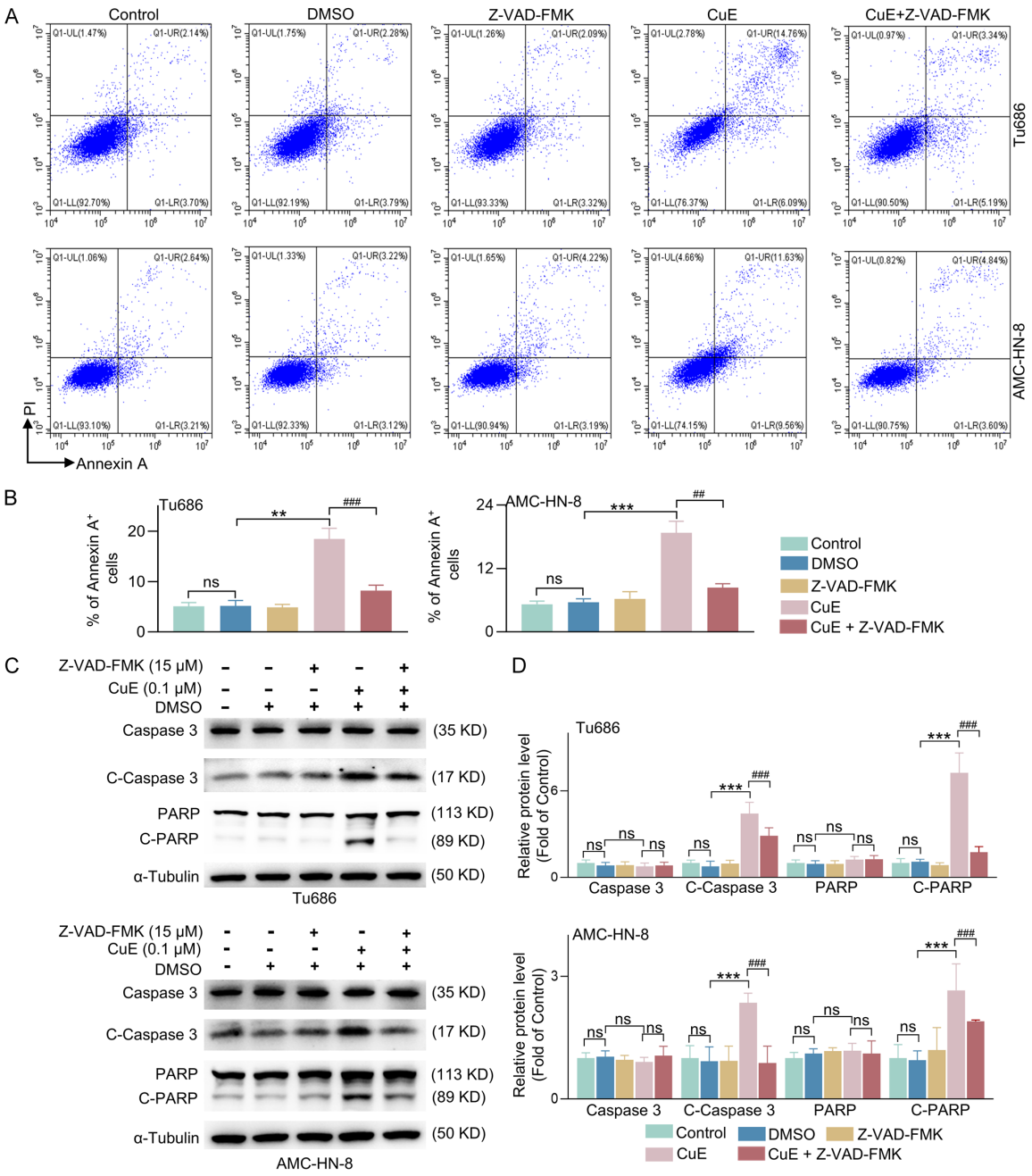

Figure 3. Z-VAD-FMK reversed the caspase-dependent apoptosis of CuE-treated LSCC cells. A, B. Flow cytometry analysis of apoptotic LSCC cells conditioned with 0.1 μM CuE for 24 h with or without 1 h of 15 μM Z-VAD-FMK pretreatment. C, D. Western blotting of C-Caspase 3/PARP in LSCC cells after 0.1 μM CuE treatment for 24 h with or without 1 h of 15 μM Z-VAD-FMK pretreatment, and the intensity of protein bands was measured using by Image J. C-Caspase 3/PARP, cleaved-Caspase 3 and cleaved-PARP. Data are presented as means ± SD (n=3). ** and *** indicate $P < 0.01$ and 0.001 *vs.* the DMSO group, respectively. ## and ### indicate $P < 0.01$ and 0.001 *vs.* the CuE group, respectively. ns, no significance.

treatment activated the p-PERK/p-eIF-2α/ATF4/CHOP signaling pathway and induced ER stress (**Figure 5B**, **5C**). To probe the impact of ER stress in CuE-triggered apoptosis, TU686 and AMC-HN-8 cells were conditioned with 4-PBA for 2 h. 4-PBA attenuated effects of CuE on p-PERK, p-eIF-2α, ATF4, and CHOP levels in LSCC cells (**Figure 6A**, **6B**) and suppressed

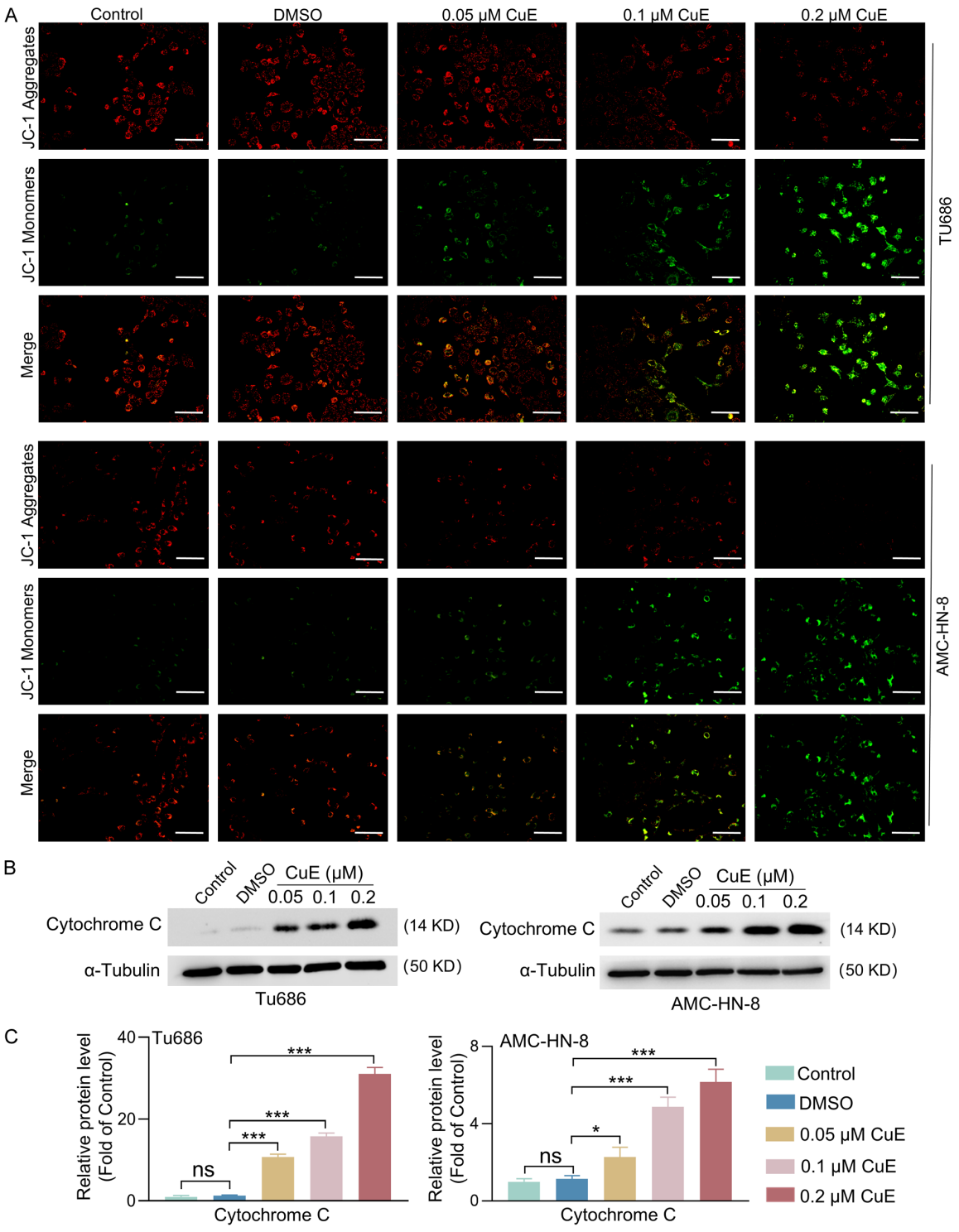

Figure 4. Functions of CuE in mitochondrial dysfunction in LSCC cells. A. JC-1 staining images of LSCC cells following CuE treatment. B, C. Western blotting of cytoplasmic cytochrome c in LSCC cells conditioned with CuE at indicated dosages for 24 h. Quantification of protein band intensity was carried out using Image J. Data are expressed as means ± SD (n=3). * and *** indicate $P < 0.05$ and 0.001 *vs.* the DMSO group. ns, no significance.

CuE-triggered apoptosis (**Figure 6C**, **6D**). These findings suggest the involvement of PERK/eIF-2α/ATF4/CHOP pathway in ER stress-triggered apoptosis in CuE-treated LSCC cells.

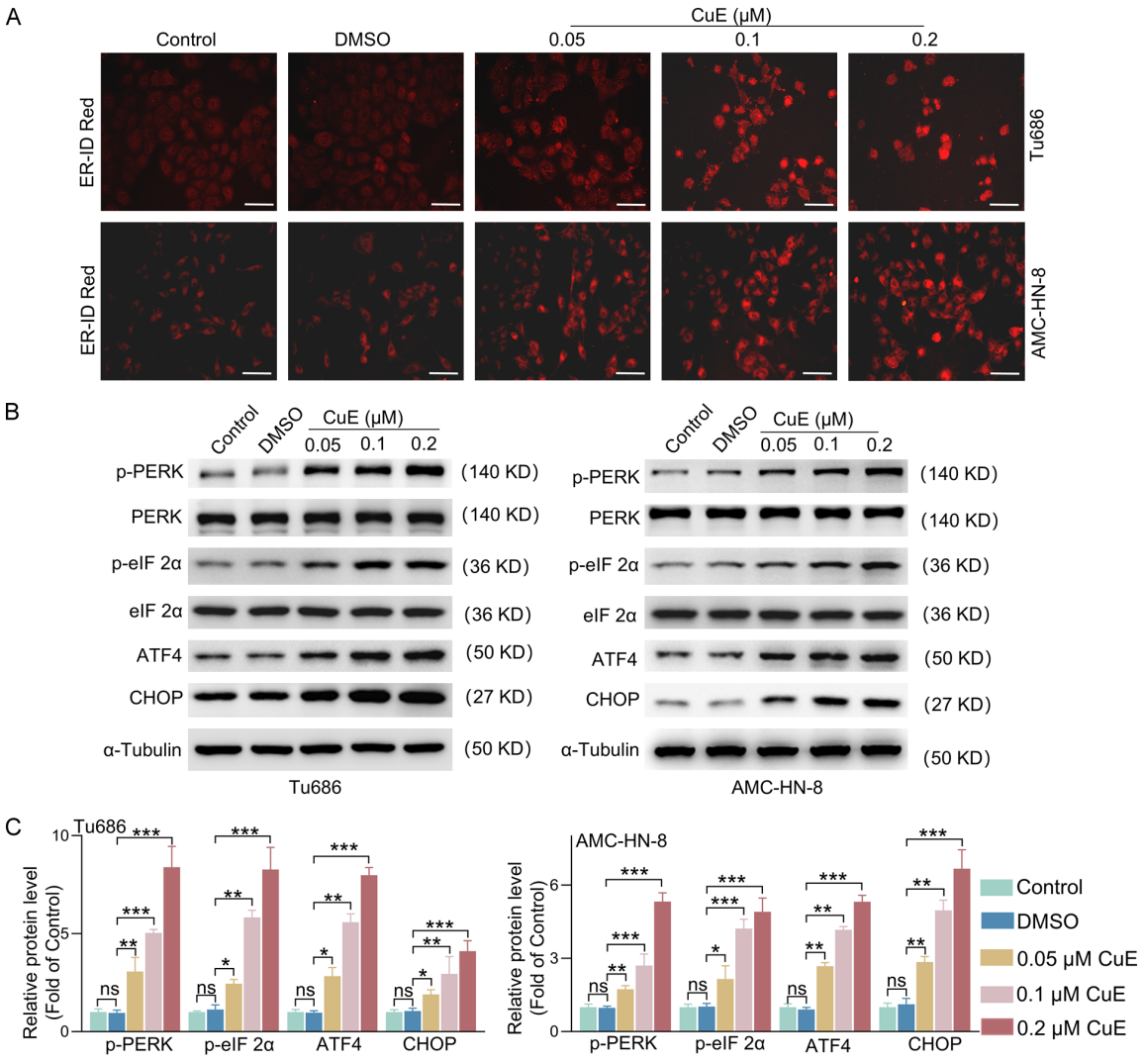

Figure 5. CuE evoked ER stress in LSCC cells. A. Immunofluorescence signals of the ER-ID red dye in CuE-treated TU686 and AMC-HN-8 cells. Scale bar =100 μm. B, C. Western blotting of p-PERK, PERK, p-eIF2α, eIF2α, ATF4, and CHOP inTU686 and AMC-HN-8 cells treated with CuE at 0.05, 0.1, and 0.2 μM for 24 h. Quantification of protein band intensity was carried out using Image J. Data are presented as means ± SD (n=3). *, **, and *** indicate $P < 0.05$, 0.01, and $P < 0.001$ *vs.* the DMSO group. ns, no significance.

CuE-mediated apoptosis and ER stress are ROS-dependent in LSCC cells

High ROS levels can induce cancer cell death [24]. To clarify whether CuE-triggered cell death was due to ROS generation, LSCC cells were reacted with varying doses of CuE for 24 h, and ROS levels were assessed using DCFH-DA staining. The results unveiled a significant, dose-dependent augmentation in cellular ROS generation in both TU686 and AMC-HN-8 cells following CuE treatment (**Figure 7A**, **7B**). To explore whether ROS serve as a signaling mediator for CuE-triggered cell death, LSCC cells were conditioned with NAC for 3 h prior to CuE treatment. Notably, NAC pretreatment reversed CuE-triggered apoptosis (**Figure 7C** and Supplementary Figure 1) and attenuated CuE's effects on cytochrome c levels in the cytoplasm (**Figure 7D**, **7E**) and C-Caspase 3/PARP levels (**Figure 7F**, **7G**). These findings suggested that CuE-triggered LSCC cell death is associated with enhanced ROS levels.

Increased ROS levels can induce apoptosis by activating pro-apoptotic pathways, including

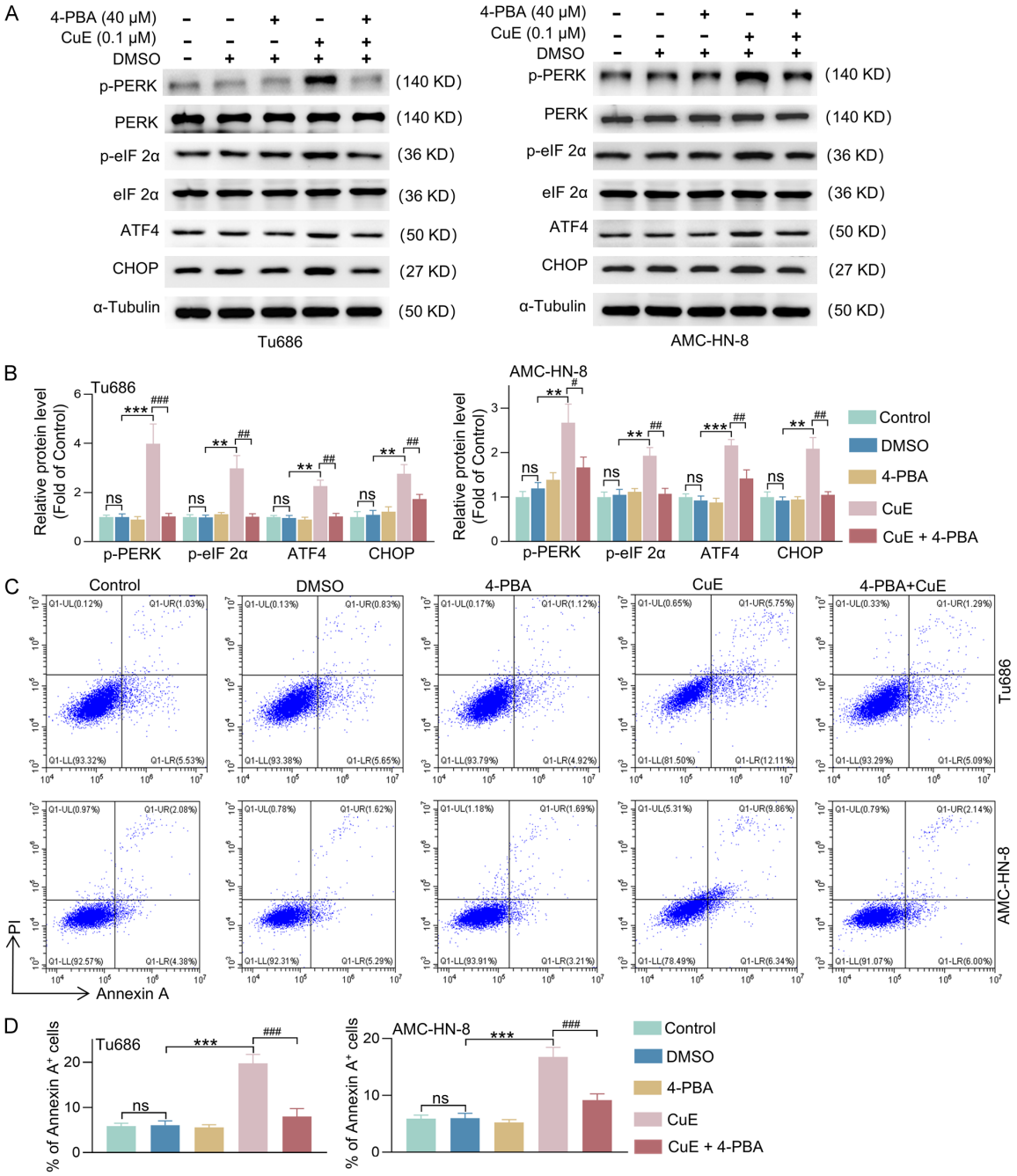

Figure 6. CuE promoted ER stress-mediated LSCC cell apoptosis. (A, B) Western blotting of p-PERK, PERK, p-eIF2α, eIF2α, ATF4, and CHOP in TU686 and AMC-HN-8 cells conditioned with 0.1 μM CuE for 24 h after preincubation with or without 40 μM 4-PBA. (C, D) Flow cytometry analyses of TU686 and AMC-HN-8 cells treated with 0.1 μM CuE for 24 h after preincubation with or without 40 μM 4-PBA. Apoptotic cells were stained with Annexin V/PI, and their proportion in each group was measured. Signals in (A) were quantified using Image J. Data are presented as means ± SD (n=3). ** and *** indicate $P < 0.01$ and 0.001 *vs.* the DMSO group, respectively. ## and ### indicate $P < 0.01$ and < 0.001 *vs.* the CuE group, respectively. ns, no significance.

ER stress-related functional disorders [25]. To investigate whether ROS function as an upstream modulators of ER stress in CuE-triggered cell death, we detected whether NAC could suppress ER stress signals. The ER-ID® Red assay revealed that NAC pretreat-

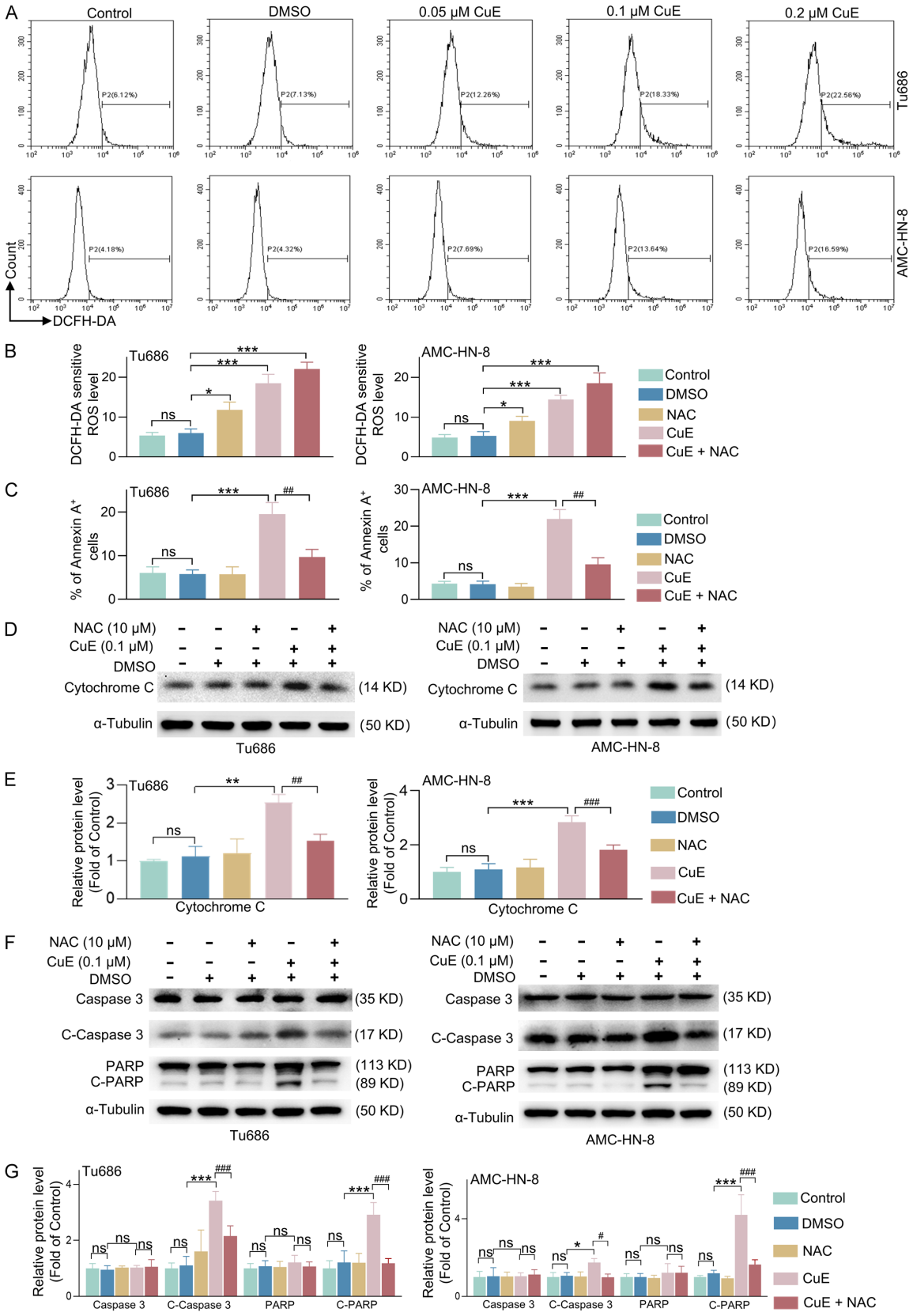

Figure 7. CuE induced ROS-mediated LSCC cell apoptosis. (A, B) Representative flow cytometry graphs and quantification of intracellular ROS levels in LSCC cells incubated with CuE at various concentrations for 24 h following

DCFH-DA staining. (C) The fraction of apoptotic LSCC cells were examined using an Annexin V/PI assay when cells were treated with CuE for 24 h after preincubation with 10 μM NAC for 3 h. (D-G) Western blotting of cytoplasmic cytochrome c (D, E) and C-Caspase 3/PARP (F, G) in cells exposed to CuE for 24 h after preincubation with 10 μM NAC for 3 h. Protein band intensity was quantified by Image J. C-Caspase 3/PARP, cleaved-Caspase 3 and cleaved-PARP. Data are expressed as means ± SD (n=3). ## and ### indicate $P < 0.01$ and 0.001 *vs.* the CuE group, respectively. *, **, and *** indicate $P < 0.05$, 0.01, and $P < 0.001$ *vs.* the DMSO group, respectively. ns, no significance.

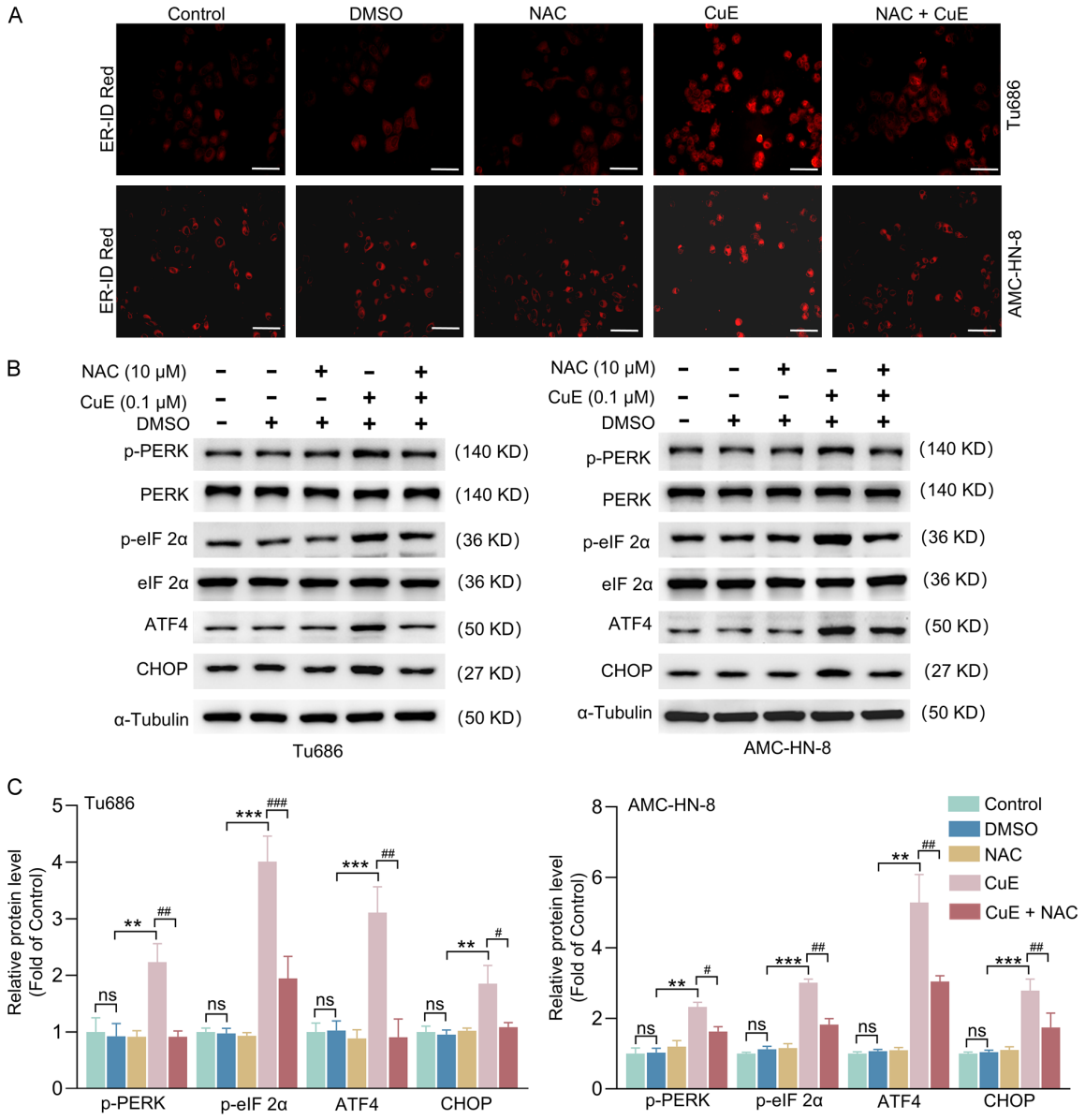

Figure 8. CuE induced ER stress-mediated LSCC cell apoptosis through the ROS pathway. A. Immunofluorescence detection of ER stress using ER-ID Red dye in NAC-pretreated, CuE-incubated TU686 and AMC-HN-8 cells. Scale bar =100 μm. B, C. Western blotting of p-PERK, PERK, p-eIF2α, eIF2α, ATF4, and CHOP in LSCC cells exposed to 0.1 μM CuE for 24 h following preincubation with or without 10 μM NAC for 3 h. Protein band intensity was quantified by Image J. All values are presented as means ± SD (n=3). ## and ### indicate $P < 0.01$ and 0.001 *vs.* the CuE group, and *, **, and *** indicate $P < 0.05$, 0.01, and $P < 0.001$ vs. the DMSO group, respectively. ns, no significance.

ment decreased fluorescent intensity in both TU686 and AMC-HN-8 cells induced by CuE treatment (**Figure 8A**), suggesting that NAC reversed CuE-induced ER stress. Moreover,

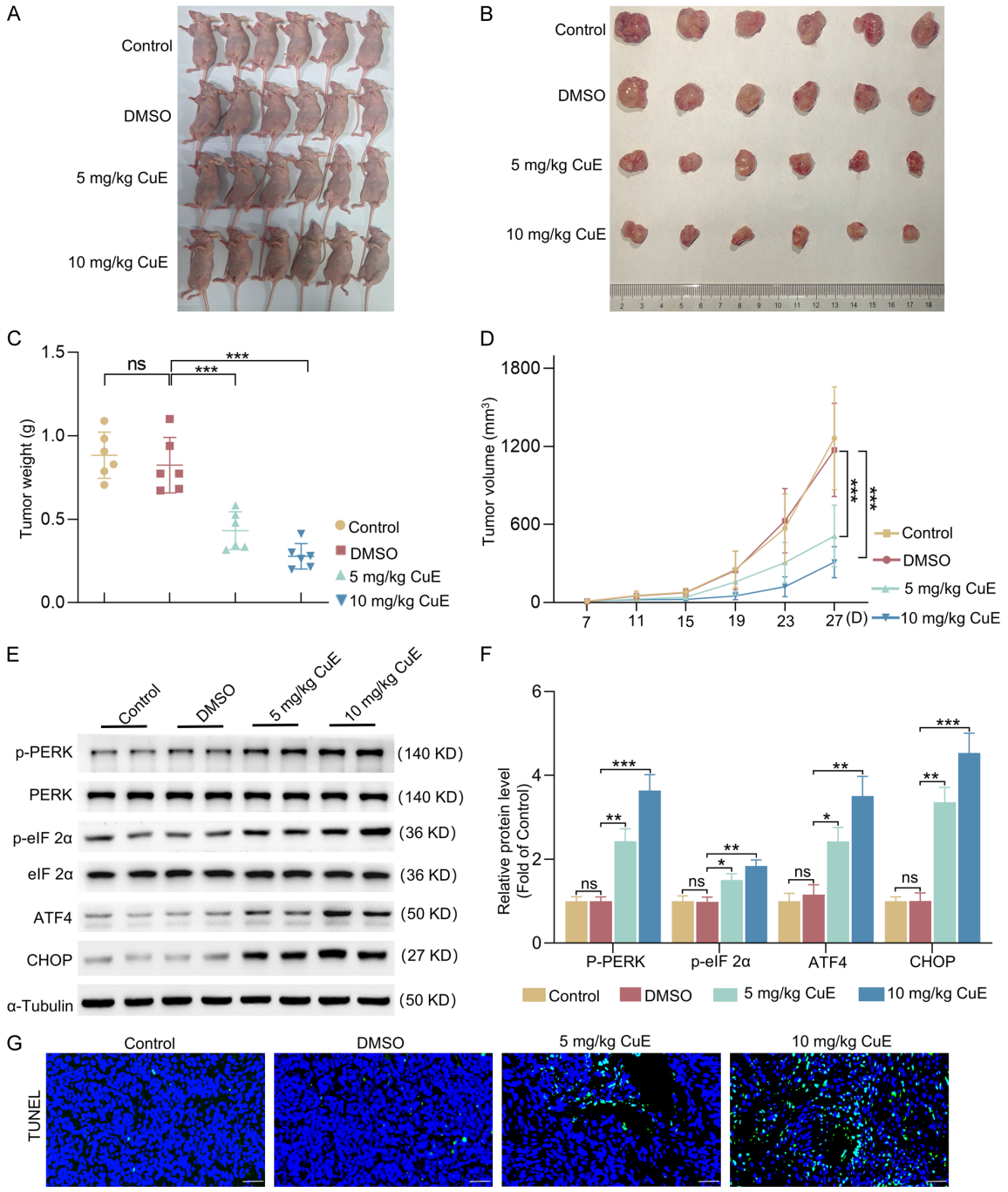

Figure 9. CuE suppressed tumor growth in mouse LSCC models usingsubcutaneous xenografts established with TU686 cells. A, B. Representative images of mice and tumors collected at the end of experiment. C, D. Changes in tumor weight and volume in the xenograft model after treatment with 5 and 10 mg/kg CuE. E, F. Western blotting of p-PERK, PERK, p-eIF2α, eIF2α, ATF4, and CHOP in tumors. The protein band intensity was quantified using Image J. G. TUNEL staining of LCSS cells in mice. Apoptotic cells and nuclei are stained green and blue, respectively. Data are presented as means ± SD, n=6/group. *, **, and *** indicate $P < 0.05$, 0.01, and $P < 0.001$ *vs.* the DMSO group, respectively. ns, no significance.

NAC pretreatment suppressed CuE-upregulated p-PERK, p-eIF-2α, ATF4, and CHOP in LSCC cells (**Figure 8B**, **8C**). These findings suggested that CuE increased ROS generation, thereby triggering ER stress and LSCC cell death.

CuE inhibits LSCC cell growth in vivo

To explore CuE's antitumor activity *in vivo*, we established a TU686 cell-derived xenograft LSCC model and treated tumor-bearing mice with CuE. Treatment with CuE significantly inhibited tumor growth (**Figure 9A**, **9B**). Moreover, the mean tumor weight and volume were reduced in the groups administered 5 mg/kg and 10 mg/kg CuE compared to the DMSO group, especially in the 10 mg/kg CuE-treated group (**Figure 9C**, **9D**). Moreover, ER stress triggered by CuE in the *in vivo* LSCC model was validated, with increased p-PERK, p-eIF-2α, ATF4, and CHOP levels after treatment with 5 and 10 mg/kg CuE, especially in the 10 mg/kg CuE group, compared to the DMSO group (**Figure 9E**, **9F**). TUNEL assays unveiled a higher number apoptotic cells in the tumor tissues of the 5 mg/kg and 10 mg/kg CuE-treated groups than in the DMSO group (**Figure 9G**). Additionally, immunohistochemistry showed no obvious morphological changes in the heart, kidney, liver, spleen, or lungs between CuE and DMSO groups (Supplementary Figure 2), indicating that CuE is relative safe *in vivo*. Taken together, these results indicate that CuE inhibited the growth of LSCC *in vivo*.

Discussion

LSCC is characterized by its high malignancy rates and ranks second in morbidity rates among patients with head and neck neoplasms [26]. Despite progress in therapeutic approaches, the 5-year survival rate of patients with LSCC remains low [27]. Therefore, there is a critical need for new antitumor agents and a deeper understanding of the molecular mechanisms underlying the inhibition of LSCC progression. This study demonstrated that CuE exerted inhibitory effects on LSCC cells, inducing excessive ER stress and mitochondrial dysfunction by elevating intracellular ROS production and triggering apoptosis. Similar results have been reported in murine LSCC models. In addition, the ROS inhibitor NAC reversed these effects. Therefore, CuE may serve as an effective candidate for treating human LSCC by inducing LSCC cell apoptosis via ROS-regulated ER stress and mitochondrial dysfunction.

ROS play a dual role in tumor cell survival [28]. Although tumor cells typically exhibit higher basal ROS levels than normal cells, a moderate increase in ROS levels facilitates tumorigenesis, metastasis, angiogenesis, and drug resistance [29-31]. Conversely, excessive ROS concentrations above threshold levels trigger various types of cell death [29]. Therefore, the modulation of intracellular ROS levels is a crucial antitumor therapeutic strategy. Several studies have indicated that some compounds such as DCZ0358, cosmosiin, and piceatannol exert their antitumor functions by inducting ROS-mediated apoptosis [32-34]. In the present study, CuE exhibited antitumor activity in LSCC cells by inducing ROS generation, which was inhibited by the antioxidant NAC. Our results suggested that ROS are the primary signal regulators of CuE-induced apoptosis.

Delving into the pro-apoptotic mechanism of CuE in detail, our data revealed that increased ROS generation led to mitochondrial dysfunction and ER stress. ER stress-mediated tumor cell apoptosis is a crucial mechanism of cancer therapeutic drugs [35, 36]. ER stress' main function is to re-establish ER homeostasis by activating the unfolded protein response. However, severe or prolonged ER stress can shift the pro-survival role to a pro-apoptotic one, triggering intrinsic apoptosis [25]. PERK/eIF2α/CHOP pathway is a prominent sensor of ER stress, inducing death upon ER stress [19]. PERK activates eIF2α, which subsequently enhances ATF4 and CHOP expression, triggering cell apoptosis [37]. Our study found that CuE dose-dependently augmented p-PERK, p-eIF2α, ATF-4, and CHOP levels, indicating that CuE induced pro-apoptotic ER stress signaling. Furthermore, pretreatment with 4-PBA partially reduced CuE-induced apoptosis, unveiling the importance of ER stress in CuE-triggered cell death. Similar to CuE, compounds such as honokiol, plumbagin, and pendulone can induce ER stress to mediate tumor cell apoptosis [19, 38, 39]. Mounting evidence supports the association between uncontrolled ROS-mediated oxidative stress and the ER stress response, leading to ER stress-dependent cell apoptosis [37, 40]. Research has unveiled that antioxidants can lower ER stress and enhance cell survival [41]. In this study, NAC blocked CuE-induced ER stress, emphasizing the role of ROS in CuE-triggered ER stress. Additionally, this ROS overproduction promotes mitochondrial membrane hyperpolarization,

causing MMP collapse, the release of cytochrome c into the cytoplasm, and caspase-dependent apoptosis [20]. Our results revealed that CuE treatment attenuated MMP and increased the cytoplasmic cytochrome c and C-Caspase 3/PARP levels in LSCC cells. Notably, NAC reversed these changes, indicating that increased ROS generation initiated ER stress by stimulating mitochondria-medicated cell death and PERK/eIF2α/CHOP pathway in CuE-stimulated LSCC cells.

Cucurbitacins, a family of plant triterpenoids, are classified into 12 categories based on their side chain structural variations [42]. CuE is the most widely distributed chemical component in this family [42]. Previous explorations have reported the potent antitumor function of CuE in colon, prostate, and lung cancer cells, as well as in hepatoma carcinoma [6, 8, 10, 43]. Our study highlights the potential role of CuE in LSCC treatment, indicating its pro-apoptotic action in LSCC cell-based systems *in vitro* and *in vivo*, and illustrates the mechanisms underlying CuE-mediated anti-LSCC activity. Overall, our study results indicated that CuE induces LCSS apoptosis by augmenting ROS-mediated mitochondrial dysfunction and ER stress and thus can serve as a valuable therapeutic agent for LSCC treatment.

Our study demonstrated that CuE has a marked inhibitory function on LSCC both *in vivo* and *in vitro*, with ROS emerging as the primary contributor to CuE's anti-LSCC activity. CuE dramatically promoted ROS generation in LSCC cells, triggering ER stress and activating PERK/eIF2α/ATK4/CHOP pathway, ultimately inducing cell apoptosis. These promising outcomes suggest that CuE has potential applications in LSCC treatment, and our data may accelerate its development toward clinical utilization.

Acknowledgements

This investigation was sponsored by the Natural Science Foundation of Anhui Province Education Department (2022AH040188), the Open Fund of Key Laboratory of Anti-inflammatory and Immune Medicine, Ministry of Education (KFJJ-2021-13), Clinical Research Project of Anhui University of Chinese Medicine (2021yfylc04), Health Research Project of Anhui Province (AHWJ2023A20149), and the 2024 Take-Off project of Shenzhen Hospital of Southern Medical University (23H3ATF01).

Disclosure of conflict of interest

None.

Address correspondence to: Huaidong Cheng, Department of Oncology, The Second Hospital of Anhui Medical University, Hefei 230601, Anhui, China. Tel: +86-13955112735; E-mail: chd1975-ay@126.com; Ling Cheng, Medical Intensive Care Unit, The First Affiliated Hospital of Anhui University of Chinese Medicine, Hefei 230031, Anhui, China. Tel: +86-0551-62850042; E-mail: chenglingnjzyy-dx@sina.com; Wei He, Department of Immunology, School of Basic Medical Sciences, Anhui Medical University, Hefei 230032, Anhui, China. Tel: +86-0551-65161139; E-mail: weihe@ahmu.edu.cn

References

[1] Wang X, Tian L, Li Y, Wang J, Yan B, Yang L, Li Q, Zhao R, Liu M, Wang P and Sun Y. RBM15 facilitates laryngeal squamous cell carcinoma progression by regulating TMBIM6 stability through IGF2BP3 dependent. J Exp Clin Cancer Res 2021; 40: 80.

[2] Steuer CE, El-Deiry M, Parks JR, Higgins KA and Saba NF. An update on larynx cancer. CA Cancer J Clin 2017; 67: 31-50.

[3] Wu Y, Zhang Y, Zheng X, Dai F, Lu Y, Dai L, Niu M, Guo H, Li W, Xue X, Bo Y, Guo Y, Qin J, Qin Y, Liu H, Zhang Y, Yang T, Li L, Zhang L, Hou R, Wen S, An C, Li H, Xu W and Gao W. Circular RNA circCORO1C promotes laryngeal squamous cell carcinoma progression by modulating the let-7c-5p/PBX3 axis. Mol Cancer 2020; 19: 99.

[4] Siegel RL, Miller KD, Wagle NS and Jemal A. Cancer statistics, 2023. CA Cancer J Clin 2023; 73: 17-48.

[5] Tang X, Tang Q, Li S, Li M and Yang T. IGF2BP2 acts as a m(6)A modification regulator in laryngeal squamous cell carcinoma through facilitating CDK6 mRNA stabilization. Cell Death Discov 2023; 9: 371.

[6] Yang P, Lian Q, Fu R, Ding GB, Amin S, Li Z and Li Z. Cucurbitacin E triggers cellular senescence in colon cancer cells via regulating the miR-371b-5p/TFAP4 signaling pathway. J Agric Food Chem 2022; 70: 2936-2947.

[7] Wang L, Xu H, Li X, Chen H, Zhang H, Zhu X, Lin Z, Guo S, Bao Z, Rui H, He W and Zhang H. Cucurbitacin E reduces IL-1beta-induced inflammation and cartilage degeneration by inhibiting the PI3K/Akt pathway in osteoarthritic chondrocytes. J Transl Med 2023; 21: 880.

[8] Liu Y, Yang H, Guo Q, Liu T, Jiang Y, Zhao M, Zeng K and Tu P. Cucurbitacin E inhibits Huh7 hepatoma carcinoma cell proliferation and

metastasis via suppressing MAPKs and JAK/STAT3 pathways. Molecules 2020; 25: 560.
[9] Si W, Lyu J, Liu Z, Wang C, Huang J, Jiang L and Ma T. Cucurbitacin E inhibits cellular proliferation and enhances the chemo-response in gastric cancer by suppressing AKt activation. J Cancer 2019; 10: 5843-5851.
[10] Jing SY, Wu ZD, Zhang TH, Zhang J and Wei ZY. In vitro antitumor effect of cucurbitacin E on human lung cancer cell line and its molecular mechanism. Chin J Nat Med 2020; 18: 483-490.
[11] Liu WB, Wang HL, Chen L, Tang B, Ke G, Wang S, Sun YQ, Ma J and Lyu DL. Cucurbitacin E inhibits cellular proliferation and induces apoptosis in melanoma by suppressing HSDL2 expression. Chin Med 2022; 17: 28.
[12] Ma G, Luo W, Lu J, Ma DL, Leung CH, Wang Y and Chen X. Cucurbitacin E induces caspase-dependent apoptosis and protective autophagy mediated by ROS in lung cancer cells. Chem Biol Interact 2016; 253: 1-9.
[13] Kong Y, Chen J, Zhou Z, Xia H, Qiu MH and Chen C. Cucurbitacin E induces cell cycle G2/M phase arrest and apoptosis in triple negative breast cancer. PLoS One 2014; 9: e103760.
[14] Lin JH, Walter P and Yen TS. Endoplasmic reticulum stress in disease pathogenesis. Annu Rev Pathol 2008; 3: 399-425.
[15] Bhat TA, Chaudhary AK, Kumar S, O'Malley J, Inigo JR, Kumar R, Yadav N and Chandra D. Endoplasmic reticulum-mediated unfolded protein response and mitochondrial apoptosis in cancer. Biochim Biophys Acta Rev Cancer 2017; 1867: 58-66.
[16] Kim TW. Nodakenin induces ROS-dependent apoptotic cell death and ER stress in radioresistant breast cancer. Antioxidants (Basel) 2023; 12: 492.
[17] Bonsignore G, Martinotti S and Ranzato E. Endoplasmic reticulum stress and cancer: could unfolded protein response be a druggable target for cancer therapy? Int J Mol Sci 2023; 24: 1566.
[18] Wu J, Wang D, Zhou J, Li J, Xie R, Li Y, Huang J, Liu B and Qiu J. Gambogenic acid induces apoptosis and autophagy through ROS-mediated endoplasmic reticulum stress via JNK pathway in prostate cancer cells. Phytother Res 2023; 37: 310-328.
[19] Lin CL, Yu CI, Lee TH, Chuang JM, Han KF, Lin CS, Huang WP, Chen JY, Chen CY, Lin MY and Lee CH. Plumbagin induces the apoptosis of drug-resistant oral cancer in vitro and in vivo through ROS-mediated endoplasmic reticulum stress and mitochondrial dysfunction. Phytomedicine 2023; 111: 154655.
[20] Redza-Dutordoir M and Averill-Bates DA. Activation of apoptosis signalling pathways by reactive oxygen species. Biochim Biophys Acta 2016; 1863: 2977-2992.
[21] Sun WC, Lin CL, Lee TH, Chang CH, Ong AZ, Yeh YH, Yu CL, Chen GW, Hsieh YH and Wang SW. Critical role of heme oxygenase-1 in chaetoglobosin A by triggering reactive oxygen species mediated mitochondrial apoptosis in colorectal cancer. Free Radic Biol Med 2023; 208: 833-845.
[22] Hsu YC, Huang TY and Chen MJ. Therapeutic ROS targeting of GADD45gamma in the induction of G2/M arrest in primary human colorectal cancer cell lines by cucurbitacin E. Cell Death Dis 2014; 5: e1198.
[23] Zhu X, Huang N, Ji Y, Sheng X, Huo J, Zhu Y, Huang M, He W and Ma J. Brusatol induces ferroptosis in oesophageal squamous cell carcinoma by repressing GSH synthesis and increasing the labile iron pool via inhibition of the NRF2 pathway. Biomed Pharmacother 2023; 167: 115567.
[24] Yan Y, Chen J, Peng M, Zhang X, Feng E, Li Q, Guo B, Ding X, Zhang Y and Tang L. Sesquiterpenes from Carpesium faberi triggered ROS-induced apoptosis and protective autophagy in hepatocellular carcinoma cells. Phytochemistry 2023; 214: 113805.
[25] Zhang X, Chen M, Zou P, Kanchana K, Weng Q, Chen W, Zhong P, Ji J, Zhou H, He L and Liang G. Curcumin analog WZ35 induced cell death via ROS-dependent ER stress and G2/M cell cycle arrest in human prostate cancer cells. BMC Cancer 2015; 15: 866.
[26] Zhu Q, Zhang R, Lu F, Zhang X, Zhang D, Zhang Y, Chen E, Han F and Zha D. Cuproptosis-related LINC02454 as a biomarker for laryngeal squamous cell carcinoma based on a novel risk model and in vitro and in vivo analyses. J Cancer Res Clin Oncol 2023; 149: 15185-15206.
[27] Zhang W, Liu T, Li X, Li T, Ma X, Zhao D and Zhao X. Increased methylation of ZNF671 suppresses tumor progression by promoting MAPK6 transcription in laryngeal carcinoma. Int J Biol Sci 2023; 19: 2443-2457.
[28] Moloney JN and Cotter TG. ROS signalling in the biology of cancer. Semin Cell Dev Biol 2018; 80: 50-64.
[29] Tuli HS, Kaur J, Vashishth K, Sak K, Sharma U, Choudhary R, Behl T, Singh T, Sharma S, Saini AK, Dhama K, Varol M and Sethi G. Molecular mechanisms behind ROS regulation in cancer: a balancing act between augmented tumorigenesis and cell apoptosis. Arch Toxicol 2023; 97: 103-120.
[30] Stieg DC, Wang Y, Liu LZ and Jiang BH. ROS and miRNA dysregulation in ovarian cancer de-

velopment, angiogenesis and therapeutic resistance. Int J Mol Sci 2022; 23: 6702.
[31] Jiang Y, Song L, Lin Y, Nowialis P, Gao Q, Li T, Li B, Mao X, Song Q, Xing C, Zheng G, Huang S and Jin L. ROS-mediated SRMS activation confers platinum resistance in ovarian cancer. Oncogene 2023; 42: 1672-1684.
[32] Çınar Ayan İ, Güçlü E, Vural H and Dursun HG. Piceatannol induces apoptotic cell death through activation of caspase-dependent pathway and upregulation of ROS-mediated mitochondrial dysfunction in pancreatic cancer cells. Mol Biol Rep 2022; 49: 11947-11957.
[33] Han JH, Lee EJ, Park W, Choi JG, Ha KT and Chung HS. Cosmosiin induces apoptosis in colorectal cancer by inhibiting PD-L1 expression and inducing ROS. Antioxidants (Basel) 2023; 12: 2131.
[34] Feng Q, Hu K, Hu H, Lu Y, Zhang H, Wang G, Zhang Q, Xu Z, Gao X, Jia X, Zhu H, Song D, Yi H, Peng Y, Wu X, Li B, Zhu W and Shi J. Berberine derivative DCZ0358 induce oxidative damage by ROS-mediated JNK signaling in DLBCL cells. Int Immunopharmacol 2023; 125: 111139.
[35] Kim C and Kim B. Anti-cancer natural products and their bioactive compounds inducing ER stress-mediated apoptosis: a review. Nutrients 2018; 10: 1021.
[36] Munoz-Guardiola P, Casas J, Megias-Roda E, Sole S, Perez-Montoyo H, Yeste-Velasco M, Erazo T, Dieguez-Martinez N, Espinosa-Gil S, Munoz-Pinedo C, Yoldi G, Abad JL, Segura MF, Moran T, Romeo M, Bosch-Barrera J, Oaknin A, Alfon J, Domenech C, Fabrias G, Velasco G and Lizcano JM. The anti-cancer drug ABTL0812 induces ER stress-mediated cytotoxic autophagy by increasing dihydroceramide levels in cancer cells. Autophagy 2021; 17: 1349-1366.
[37] Wang X, Guo Q, Tao L, Zhao L, Chen Y, An T, Chen Z and Fu R. E platinum, a newly synthesized platinum compound, induces apoptosis through ROS-triggered ER stress in gastric carcinoma cells. Mol Carcinog 2017; 56: 218-231.
[38] Cheng WC, Wen Y, Chiu YS, Chou CH, Lim CJ, Lin SH, Chang JM and Lin CC. Pendulone induces apoptosis via the ROS-mediated ER-stress pathway in human non-small cell lung cancer cells. Toxicol In Vitro 2022; 81: 105346.
[39] Zhu J, Xu S, Gao W, Feng J and Zhao G. Honokiol induces endoplasmic reticulum stress-mediated apoptosis in human lung cancer cells. Life Sci 2019; 221: 204-211.
[40] Yang Y, Liu Y, Zhang Y, Ji W, Wang L and Lee SC. Periplogenin activates ROS-ER stress pathway to trigger apoptosis via BIP-eIF2alpha-CHOP and IRE1alpha-ASK1-JNK signaling routes. Anticancer Agents Med Chem 2021; 21: 61-70.
[41] Malhotra JD, Miao H, Zhang K, Wolfson A, Pennathur S, Pipe SW and Kaufman RJ. Antioxidants reduce endoplasmic reticulum stress and improve protein secretion. Proc Natl Acad Sci U S A 2008; 105: 18525-18530.
[42] Yang P, Liu W, Fu R, Ding GB, Amin S and Li Z. Cucurbitacin E chemosensitizes colorectal cancer cells via mitigating TFAP4/Wnt/beta-catenin signaling. J Agric Food Chem 2020; [Epub ahead of print]
[43] He X, Gao Q, Qiang Y, Guo W and Ma Y. Cucurbitacin E induces apoptosis of human prostate cancer cells via cofilin-1 and mTORC1. Oncol Lett 2017; 13: 4905-4910.

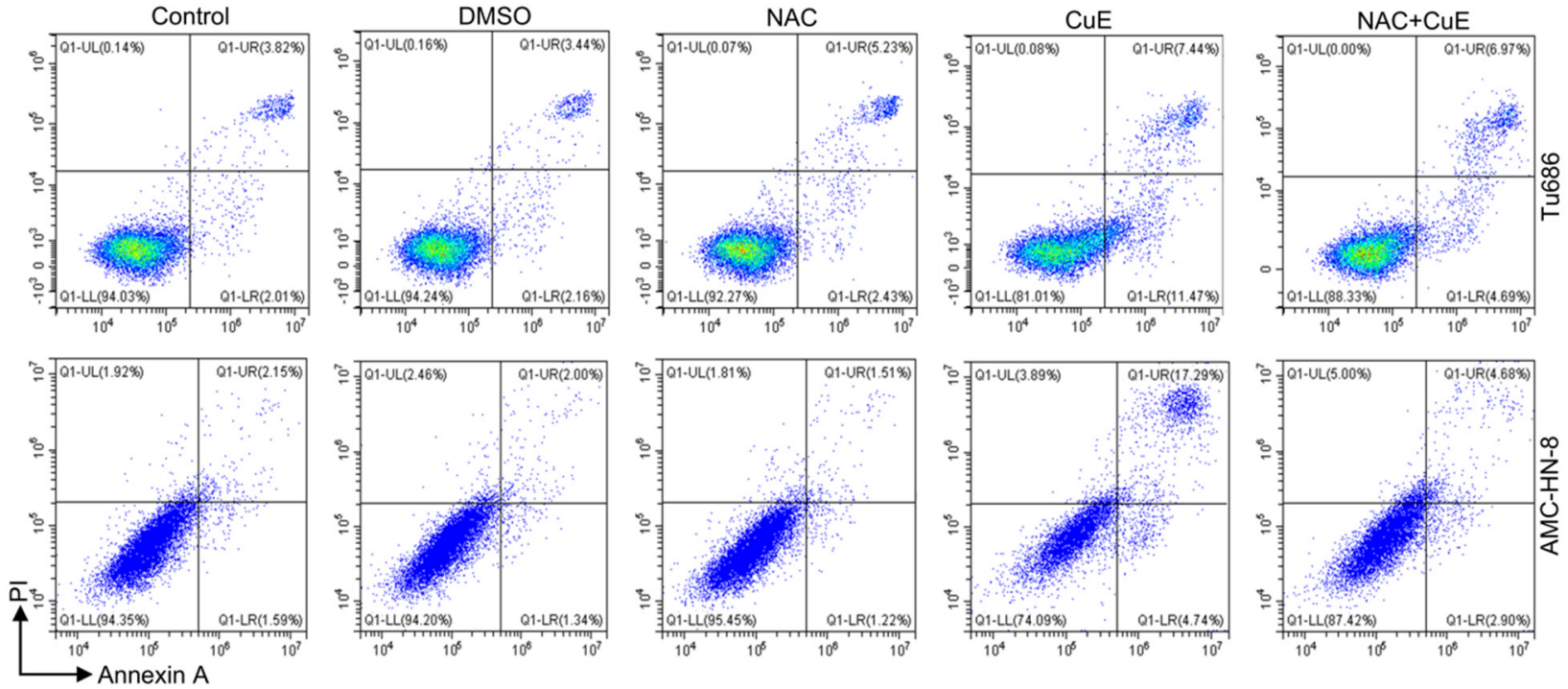

Supplementary Figure 1. NAC blocked CuE-induced apoptosis in LSCC cells. Representative flow cytometric graphs of apoptotic LSCC cells when cells were incubated with CuE for 24 h after preincubation with 10 μM NAC for 3 h (n=3).

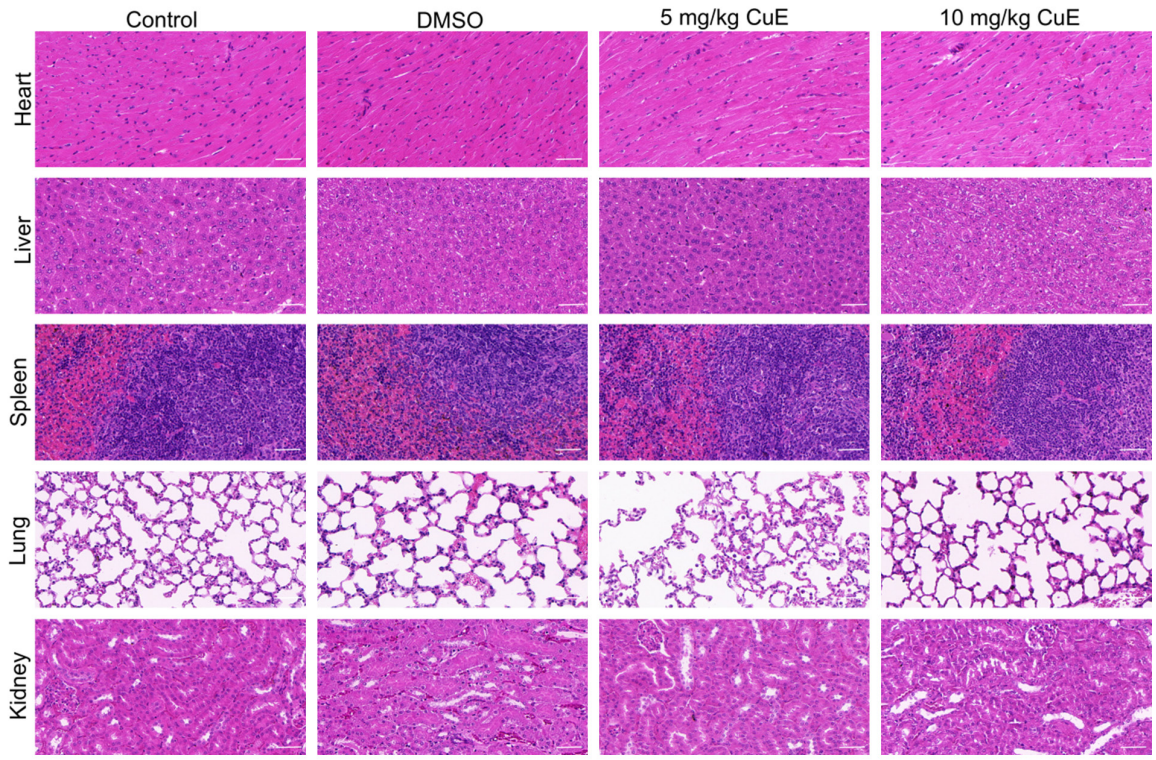

Supplementary Figure 2. H&E staining of heart, liver, spleen, lung, and Kidney from Control, DMSO, 5 mg/kg, and 10 mg/kg group. Scale bar =100 μm. n=6/group.